JOURNAL OF AIRCRAFT
Vol. 46, No. 5, September–October 2009

Unified Flutter Solution Technique Using Matrix Singularity Indicators

Zhichun Yang* and Yingsong Gu†
Northwestern Polytechnical University, 710072 Xi'an, People's Republic of China

DOI: 10.2514/1.37985

Conventional linear flutter analysis using the *k* or *p-k* method is based on eigenvalue solution of the flutter equation, which needs to track the eigenmodes to give a proper flutter point, but sometimes the procedure may fail. As a step toward a flutter solution method with more automation and robustness, a discussion is made for the uniqueness of the flutter matrix singularity at and inside the flutter boundary, and proper clearance procedure against nonuniqueness is provided. Four indicators of matrix singularity are introduced: that is, the determinant module, minimum module eigenvalue, minimum singular value, and inverse condition number of the flutter matrix. Finally, a unified algorithm is developed for flutter solution with these indicators. Numerical examples demonstrated that the results by the present method coincide well with the *p-k* and *k* methods but need no mode tracking. It is also shown that the coupled flutter-mode information can be extracted qualitatively from frequency diagrams of these indicators at different velocities and quantitatively from the eigenvector corresponding to the minimum module eigenvalue of the flutter matrix at the critical flutter point.

Nomenclature

$\boldsymbol{B}$	=	generalized damping matrix
b	=	semichord, ft
$\boldsymbol{K}$	=	generalized stiffness matrix
k	=	reduced frequency
$\boldsymbol{M}$	=	generalized mass matrix
$\boldsymbol{\eta}$	=	generalized displacement coordinates
n	=	number of modes incorporated in the aeroelastic model
$\boldsymbol{Q}$	=	generalized aerodynamic influence coefficient matrix
q_∞	=	dynamic pressure, $1/2\rho_\infty V^2$
s	=	Laplace variable
V	=	velocity, ft/s
V_F, V_f	=	theoretical and calculated flutter speed, ft/s
ρ_∞	=	air density, lb/in.^{3}
ω	=	frequency, rad/s
ω_F, ω_f	=	theoretical and calculated flutter frequency, rad/s

Introduction

LINEAR flutter analysis is now very mature in the aeroelastic research field. There are two classical flutter solution methods: namely, the *k* method developed by Theodorsen [1] and the *p-k* method by Hassig [2]. Both are widely used in aeronautical engineering and well documented in texts of aeroelasticity [3,4], but the *p-k* method is usually favored because it can give a damping factor that is physically meaningful, as opposed to the artificial damping term introduced by the *k* method. In recent years, a true damping solution technique, called the *g* method, was proposed by Chen [5], which can obtain unlimited roots. The *p-k* method has to solve for the eigenvalues of flutter equation iteratively and it tracks eigenmodes to give the proper flutter result. Such a procedure may become very critical when two aeroelastic modes have quite close frequencies, which is sometimes called the branch-crossing problem [6]. The situation can be quite difficult in real-world problems, especially the multidisciplinary-optimization (MDO) environment [7], in which mode tracking is not always effective and human interaction is usually needed to validate the results such as the *V–g* diagrams. This is tedious work and may make the optimization an impossible job.

Afolabi [8] developed a new flutter analysis approach using transversality theory with mathematical insight to aeroelastic instability. According to Afolabi's theory, the discriminant of the characteristic polynomial vanishes at the flutter point with the occurrence of degenerate eigenvalues. This conclusion strictly depends on the expression of steady aerodynamics, because the discussion is limited to the characteristic polynomial with all real coefficients, but unsteady aerodynamics employed for general wing surface are always complex in the frequency domain. Hence, the discriminant may not be zero in such cases.

It is found for specific aeroelastic stability problems, such as panel flutter in supersonic flow, that the orientations of flutter eigenvectors can be used to predict the flutter point; namely, the angle between two eigenvectors decreases to zero and hence indicates flutter [9]. More recently, this approach was employed in flutter prediction for control law design in a flutter suppression study with piezoelectric layers [10]. However, this method may suffer the same problem as that described in [8] in general aeroelastic applications, such as wing or tail flutter solutions.

The preceding flutter solution methods are based on either eigenvalue or eigenvector orientations, and there are still other approaches using only matrix singularities. Matrix singular value approach was demonstrated as a powerful tool in the multivariable feedback system stability analysis [11] and it was later applied to study the stability margin of a multiloop flutter suppression system [12]. Furthermore, it was also adopted to evaluate the performance of control system in companion with the determinant and minimum module eigenvalue of the return difference matrix [13,14]. The determinant of the flutter matrix was introduced as a flutter indicator by Banerjee [15], and it was later integrated into an aeroelastic optimization routine [16]. The concept is very insightful; that is, the flutter determinant vanishes when flutter occurs.

Singularity of the flutter matrix is a global indicator of the flutter point, which is independent of any specific mode explicitly. In this effort, a discussion is first conducted to ensure uniqueness of such singularity at and inside the flutter boundary with proper clearance procedure against nonuniqueness problems, which makes it possible to develop a simple and robust flutter solution technique without branch-crossing problems. Four singularity indicators are presented

Received 9 April 2008; revision received 9 June 2009; accepted for publication 5 June 2009.

*Professor, School of Aeronautics, P.O. Box 118, Youyi Xilu No. 127; yangzc@nwpu.edu.cn. Member AIAA.

†Ph.D. Candidate, School of Aeronautics, P.O. Box 118, Youyi Xilu No. 127. Student Member AIAA.

as a generalization of the approach in [11–16]: that is, the determinant module, minimum module eigenvalue, minimum singular value, and inverse condition number of the flutter matrix. Such indicators are all nonnegative real values and they will decrease to a global minimum zero at the flutter point. A unified algorithm with these four indicators is given and it is demonstrated to be very useful in frequency-domain flutter analysis.

Modal Flutter Equation

The focus of this study is on the flutter solution method, and so we directly introduce the modal flutter equation in the Laplace domain:

$$(s^2\boldsymbol{M} + s\boldsymbol{B} + \boldsymbol{K})\boldsymbol{\eta} - q_\infty \boldsymbol{Q}(s)\boldsymbol{\eta} = 0 \tag{1}$$

where $\boldsymbol{M}, \boldsymbol{B}, \boldsymbol{K} \in \boldsymbol{R}^{n\times n}$, and $\boldsymbol{\eta} \in \boldsymbol{C}^{n\times n}$. Because panel aerodynamics in the frequency domain is mostly available for subsonic or supersonic flow, the frequency-domain flutter equation is usually preferable in routine analysis. Now let $s = i\omega$ and $k = \omega b/V$, and then one obtains the following equation from Eq. (1):

$$[-\omega^2\boldsymbol{M} + i\omega\boldsymbol{B} + \boldsymbol{K} - q_\infty \boldsymbol{Q}(ik)]\boldsymbol{\eta} = 0 \tag{2}$$

where $\boldsymbol{Q}(ik)$ is the generalized aerodynamic influence coefficient (GAIC) matrix in the frequency domain.

Hence, the frequency-domain flutter matrix can be defined as

$$\boldsymbol{F}(V, \omega) = -\omega^2\boldsymbol{M} + i\omega\boldsymbol{B} + \boldsymbol{K} - q_\infty \boldsymbol{Q}(ik) \tag{3}$$

which is a complex function matrix of variables V and ω, but it is not a Hermitian matrix (i.e., $\boldsymbol{F} \neq \boldsymbol{F}^H$). Assuming $\boldsymbol{Q}(ik)$ is a continuous function matrix of k, then $\boldsymbol{F}$ would be also a continuous function matrix of variables V and ω.

Now it is necessary to make a comparison of the current frequency-domain flutter matrix with that in the classical p, k, and p-k methods. The p method is actually a Laplace domain (p domain) method [5]. Replacing the Laplace variable s with the nondimensional Laplace variable $p = sb/V$ in Eq. (1), one obtains

$$(\boldsymbol{M}p^2V^2/b^2 + \boldsymbol{B}pV/b + \boldsymbol{K})\boldsymbol{\eta} - q_\infty \boldsymbol{Q}(pV/b)\boldsymbol{\eta} = 0 \tag{4}$$

Hence, the flutter matrix can be derived from the p method as the following:

$$\boldsymbol{F} = \boldsymbol{M}p^2V^2/b^2 + \boldsymbol{B}pV/b + \boldsymbol{K} - q_\infty \boldsymbol{Q}(pV/b) \tag{5}$$

The approximate flutter equation in the k method [1] reads

$$[-\omega^2\boldsymbol{M} + i\omega\boldsymbol{B} + (1 + ig)\boldsymbol{K} - q_\infty \boldsymbol{Q}(ik)]\boldsymbol{\eta} = 0 \tag{6}$$

The associated flutter matrix can be directly written as

$$\boldsymbol{F} = -\omega^2\boldsymbol{M} + i\omega\boldsymbol{B} + (1 + ig)\boldsymbol{K} - q_\infty \boldsymbol{Q}(ik) \tag{7}$$

Finally, the approximate flutter equation and the flutter matrix of the p-k method modified by Rodden and Johnson [17] can be expressed as

$$[\boldsymbol{M}s^2 + (\boldsymbol{B} - \tfrac{1}{2}\rho_\infty bV\boldsymbol{Q}(ik)^I/k)s + (\boldsymbol{K} - q_\infty \boldsymbol{Q}(ik)^R)]\boldsymbol{\eta} = 0 \tag{8}$$

and

$$\boldsymbol{F} = \boldsymbol{M}s^2 + (\boldsymbol{B} - \tfrac{1}{2}\rho_\infty bV\boldsymbol{Q}(ik)^I/k)s + (\boldsymbol{K} - q_\infty \boldsymbol{Q}(ik)^R) \tag{9}$$

respectively.

It is found that the flutter matrices within these classical methods will reduce to the same expression with the frequency-domain flutter matrix in Eq. (3) along the image axis in the complex plane (i.e., $g = 0$ or $s = i\omega$). Therefore, only the frequency-domain flutter matrix would be sufficient to describe the critical flutter condition.

The frequency-domain flutter equation (2) has a compact form for the flutter matrix defined in Eq. (3): namely,

$$\boldsymbol{F}\boldsymbol{\eta} = 0 \tag{10}$$

It is concluded from linear algebra theory that Eq. (10) has a nontrivial solution if, and only if,

$$\det \boldsymbol{F} = 0 \tag{11}$$

It is well known that the flutter determinant will vanish at the flutter point. Hence, Eq. (11) is valid at the critical flutter point: namely,

$$\det \boldsymbol{F}(V_F, \omega_F) = 0 \tag{12}$$

From a mathematical point of view, Eq. (12) also means that $\boldsymbol{F}$ is singular at the flutter point. This singularity may be applied to determine the flutter point as performed in [15,16]. However, the uniqueness of such singularity should be determined first before taking it as the flutter indicator, because Eq. (11) is only a necessary condition for flutter, but it is not a sufficient condition.

Uniqueness of the Flutter Matrix Singularity

Singularity of the flutter matrix must be unique to determine a correct flutter point. If $\boldsymbol{F}$ becomes singular at other points inside the flutter boundary, then such singularity indicator would be ineffective in the flutter solution. To the authors' knowledge, two specific cases do exist: rigid-body mode and in-plane mode in the aeroelastic model can make Eq. (11) valid at two certain frequency points, respectively.

Rigid-Body Mode

For rigid-body mode, the associated column of the generalized stiffness matrix has all-zero entries. And there would be no aerodynamic effect on this mode at a steady state (i.e., $\omega = 0$) if it only has translational displacement (e.g., vertical or lateral motion). Hence, the entire column associated with this mode should be zero in the GAIC matrix $\boldsymbol{Q}$. It is observed obviously from Eq. (3) that the flutter matrix will have an all-zero column with respect to such rigid-body mode at zero frequency [i.e., $\det \boldsymbol{F}(V, 0) = 0$].

Neither modal damping nor artificial damping is applicable to prevent such singularity at $\omega = 0$, because it is a zero-frequency mode and the corresponding generalized stiffness is also zero. To consider the coupling of rigid-body mode in the flutter solution, but avoid such nonunique singularity, an alternative way is to set the frequency band analyzed well above zero. The lowest frequency is set to about one-tenth of the first elastic modal frequency in the following numerical examples. This choice is reasonable in real cases because dynamic instability always corresponds to some nonzero frequency.

In-Plane Mode

In-plane mode usually arises in aerodynamic structures such as a large-aspect-ratio wing with heavy stores, which is also called sway mode or fore–aft mode. It is an elastic mode but scarcely affects any aerodynamics in the aeroelastic motion. Theoretically, the entire column of the GAIC matrix $\boldsymbol{Q}$ associated with the in-plane mode would be zero at each frequency point.

If the generalized damping matrix is not included in Eq. (3), the flutter determinant will also be zero at different velocities right at the natural frequency of the in-plane mode, $\omega = \omega_{\text{in}}$ [i.e., $\det \boldsymbol{F}(V, \omega_{\text{in}}) = 0$], because the dynamic stiffness matrix will also have an all-zero column for this mode. Just adding some modal damping will be sufficient to prevent such singularity.

Note that the in-plane mode still remains a problem and it is sometimes suggested to be removed in flutter analysis [7]. Maybe it is also a main source that alters the automation process of the flutter solution in addition to the branch-crossing problem. Meanwhile, if the flutter determinant module holds a minimum at the same frequency point corresponding to a specific elastic mode at various velocities, then one has to check its mode shape to see whether it is an in-plane mode, and some damping may need to be added to prevent such phenomenon.

After the clearance procedure for the nonuniqueness of the singularity, Eq. (11) would be a necessary and sufficient condition for

flutter. More assumptions still need to be introduced to make $\det \boldsymbol{F}$ a unique indicator of flutter:

1) Critical flutter speed V_F is a single value function of variable ω_F.

2) Critical flutter frequency ω_F is a single value function of variable V_F.

Based on assumptions 1 and 2, it is concluded that only one pair of V_F and ω_F in the V–ω parametric plane satisfies Eq. (11) and, in the next section, four indicators will be introduced to determine the critical flutter point.

Singularity Indicators of the Flutter Matrix

Flutter Determinant Module

Because $\det \boldsymbol{F}$ is usually complex, its module $|\det \boldsymbol{F}| \geq 0$ is numerically preferable as an indicator. With this indicator, a lemma can be derived from the preceding assumptions.

Lemma 1: Given $\mathrm{d}V > 0$, if $V \in (0, V_F + \mathrm{d}V]$, then

$$|\det \boldsymbol{F}(V, \omega)|_{\min} = |\det \boldsymbol{F}(V_F, \omega_F)| = 0$$

where $\mathrm{d}V$ is augmented to make the flutter point fall into the computing velocity interval, and ω will sweep over the structural modal frequencies incorporated in the flutter solution.

Lemma 1 is a direct result from Eq. (12) and assumptions 1 and 2, which means a global minimum, $|\det \boldsymbol{F}|_{\min}$, in the V–ω parametric plane. This unique property makes it possible to determine the flutter speed by just searching for $|\det \boldsymbol{F}|_{\min}$ among a set of frequency points at varied velocities.

Indicator $|\det \boldsymbol{F}| = 0$ is not the only descriptor of the flutter matrix singularity. There are other three singularity indicators in hand: the minimum module eigenvalue, the minimum singular value, and the inverse condition number of the flutter matrix. Each of them is followed by a lemma, as shown subsequently.

Minimum Module Eigenvalue

The eigenvalues of non-Hermitian matrix $\boldsymbol{F}$ read $\lambda_1, \lambda_2, \ldots, \lambda_n$ in decreasing magnitude order. They usually include complex values. It is known from linear algebra theory that

$$\det \boldsymbol{F} = \lambda_1 \lambda_2 \cdots \lambda_n \tag{13}$$

and the modules for both sides of Eq. (13) have a relationship noted as

$$|\det \boldsymbol{F}| = |\lambda_1| \cdot |\lambda_2| \cdots |\lambda_n| \geq |\lambda_n|^n \geq 0 \tag{14}$$

Hence, $\det \boldsymbol{F} = 0 \Leftrightarrow \lambda_n = 0$. Combined with Lemma 1, one obtains Lemma 2.

Lemma 2: Given $\mathrm{d}V > 0$, if $V \in (0, V_F + \mathrm{d}V]$, then

$$|\lambda_n \boldsymbol{F}(V, \omega)|_{\min} = |\lambda_n \boldsymbol{F}(V_F, \omega_F)| = 0$$

As stated in Lemma 2, $|\lambda_n \boldsymbol{F}|$ also has a global minimum at the flutter point in the V–ω parametric plane. Therefore, it is also an indicator for the flutter matrix singularity.

Minimum Singular Value

Singular values are nonnegative real values for non-Hermitian matrix $\boldsymbol{F}$ (i.e., $\sigma_1, \sigma_2, \ldots, \sigma_n$ in decreasing order). It is known from matrix singularity theory that

$$\det \boldsymbol{F} = 0 \Leftrightarrow \sigma_n = 0 \tag{15}$$

Thus, σ_n becomes a flutter indicator and the following lemma can be written.

Lemma 3: Given $\mathrm{d}V > 0$, if $V \in (0, V_F + \mathrm{d}V]$, then

$$\sigma_n \boldsymbol{F}(V, \omega)_{\min} = \sigma_n \boldsymbol{F}(V_F, \omega_F) = 0$$

Inverse Condition Number

Matrix condition number can also describe singularities, which has several types of definitions. Perhaps the 2-norm condition number is the most widely used one: namely,

$$\mathrm{cond}\,(\boldsymbol{F}) = \sigma_1 / \sigma_n \geq 0 \tag{16}$$

At the critical flutter point, singularity occurs, and $\mathrm{cond}(\boldsymbol{F}) = \infty$ becomes a theoretical maximum. To transform it into a minimum such as the other indicators, the inverse condition number is introduced:

$$\mathrm{cond}^{-1}(\boldsymbol{F}) = \sigma_n / \sigma_1 \geq 0 \tag{17}$$

Note that

$$\det \boldsymbol{F} = 0 \Leftrightarrow \sigma_n = 0 \Leftrightarrow \mathrm{cond}^{-1}(\boldsymbol{F}) = 0$$

also indicates flutter, and thus the corresponding lemma reads as follows.

Lemma 4: Given $\mathrm{d}V > 0$, if $V \in (0, V_F + \mathrm{d}V]$, then

$$\mathrm{cond}^{-1} \boldsymbol{F}(V, \omega)_{\min} = \mathrm{cond}^{-1} \boldsymbol{F}(V_F, \omega_F) = 0$$

From complex analysis theory [18], all of these four indicators (i.e., $|\det \boldsymbol{F}|$, $|\lambda_n \boldsymbol{F}|$, $\sigma_n \boldsymbol{F}$, and $\mathrm{cond}^{-1} \boldsymbol{F}$) are continuous functions of matrix $\boldsymbol{F}$, and they are also continuous with respect to variables $V > 0$ and $\omega > 0$. Such indicators will converge to zero theoretically, but they will hardly be zero in numerical computations. Therefore, a search for their minimum values is of more importance in flutter-point determination.

It seems that $|\det \boldsymbol{F}|$ and $\mathrm{cond}^{-1} \boldsymbol{F}$ are more general singularity indicators than $|\lambda_n \boldsymbol{F}|$ and $\sigma_n \boldsymbol{F}$ in their mathematical definitions, whereas indicators based on matrix singular value would be of more confidence in the singularity evaluation of the flutter matrix. However, all of these indicators would have good performance in singularity detection for a continuously varied matrix $\boldsymbol{F}$, because they all theoretically share the same minimum at the critical flutter point.

Unified Algorithm

As stated previously, each of these four indicators is applicable in flutter solution and they will get a global minimum at the flutter point. Therefore, a unified algorithm will be sufficient to find a flutter solution by using each of these indicators.

Because the singularity indicators are multivariable functions of parameters V and ω, the strategy to search for the minimum of an indicator is, for instance, given an initial velocity $V^{(m)}$, to compute the indicator [e.g., $|\det \boldsymbol{F}(V^{(m)}, \omega)|$] in the frequency domain to find the smallest magnitude and corresponding frequency [i.e., respectively, $|\det \boldsymbol{F}(V^{(m}, \omega)|_{\min}$ and $\omega^{(m)}$] and then increase the velocity to $V^{(m+1)} = V^{(m)} + \mathrm{d}V$. Repeat this process until the occurrence of an abrupt drop (i.e., catastrophe [8]) of $|\det \boldsymbol{F}|_{\min}$ along the velocity axis. It indicates that the flutter point just falls within the neighbor region of the corresponding pair of parameters. A bisection search is then executed in this region to find the smallest $|\det \boldsymbol{F}|_{\min}$ and the associated pair of V and ω until a preset convergence accuracy is satisfied.

Numerically, the indicator will feature a catastrophe (i.e., a local minimum near the flutter point with a refined velocity set and a dense-enough frequency grid), which cannot always be guaranteed to be a global minimum. This is rather an obstacle in the searching process and, alternatively, a local minimum of $|\det \boldsymbol{F}|_{\min}$ near the flutter speed may be numerically more available and realistic.

Physically speaking, as the velocity increases, an aerodynamic surface is usually stable up to a maximum stability level, at certain velocity, due to the aerodynamic damping (see [4,5] about the aerodynamic damping matrix), and later destabilized to become unstable toward the flutter point due to the aeroelastic coupling effect. This fact would also reflect changes in its mathematical model, which implies that a state with less stability would correspond to a smaller indicator for an aeroelastic system. In this situation, the flutter indicator behaves in a similar fashion to damping, although it is not damping.

It is assumed that a smaller indicator implies a lower damping level for an aeroelastic system. Based on this assumption, singularity

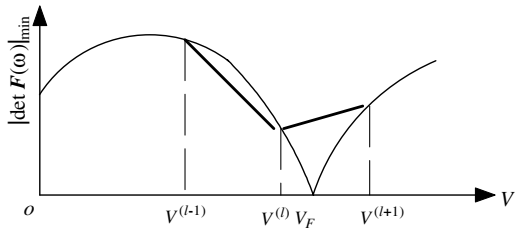

Fig. 1 Diagram of $|\det \boldsymbol{F}|_{\min}$ vs velocity under the assumption of only one local minimum.

indicators would increase up to a maximum as velocity increases, later decrease to a minimum near the flutter speed, and then increase again above the flutter speed. This conclusion guarantees that only one local minimum exists, just around the flutter speed. In this fashion, the searching approach can gain more automation. Still taking $|\det \boldsymbol{F}|$ as an example, and combined with the primary discussions at the beginning of this section, a unified algorithm is developed, and a sketch for the indicator is shown in Fig. 1.

Unified Algorithm

Compute $|\det \boldsymbol{F}(V^{(m)}, \omega)|$ in the frequency domain at a given velocity, $V^{(m)}$, and obtain $|\det \boldsymbol{F}(V^{(m)}, \omega)|_{\min}$. Repeat this process at a set of increasing velocities until the first local minimum of $|\det \boldsymbol{F}|_{\min}$ is met along the velocity axis. Then the corresponding pair of $V^{(l)}$ and $\omega^{(l)}$ indicates that the flutter speed is in the interval of $V^{(l-1)}$ and $V^{(l+1)}$. A bisection search is then executed within this interval to find the smallest $|\det \boldsymbol{F}|_{\min}$ and the associated pair of V_F and ω_F until a certain accuracy level is satisfied.

As noted in Fig. 1, the fine line is just a theoretical diagram, especially for the indicator at V_F, because a coarse velocity set is usually used in routine flutter analysis. Therefore, the thick line is more meaningful in real cases that use this algorithm.

If there are other local minima of $|\det \boldsymbol{F}|_{\min}$ inside the flutter boundary, as shown by the short dashed lines in Fig. 2, then a criterion needs to be introduced to determine the effective local minimum as a supplement to the unified algorithm. Because the catastrophe of singularity indicators only occurs at the flutter point, a threshold can be set for the unified algorithm to make a local minimum that indicates flutter only at the occurrence of a sharp-enough, or abrupt-enough, change in its magnitude: for example,

$$\max\{|\det \boldsymbol{F}(V^{(1)})|_{\min}, |\det \boldsymbol{F}(V^{(2)})|_{\min}, \ldots, |\det \boldsymbol{F}(V^{(l+1)})|_{\min}\}/|\det \boldsymbol{F}(V^{(l)})|_{\min} > 2 \tag{18}$$

which means that the magnitude of an effective local minimum should be less than half of the maximum of $|\det \boldsymbol{F}(V^{(m)})|_{\min}$ $(m = 1, 2, \ldots, l+1)$. This is a fail-safe mode for the unified algorithm and still far from covering all different situations in real problems, but it would be still effective with a refined velocity set and a dense-enough frequency grid.

Actually, it is found that a dense-enough frequency grid would ensure that the first local minimum of $|\det \boldsymbol{F}|_{\min}$ indicates flutter, and it would also be the only local minimum around the flutter speed. Hence, the fail-safe mode may only be activated when a relatively coarse frequency grid is used in the unified algorithm.

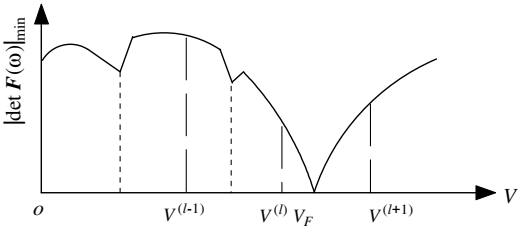

Fig. 2 Diagram of $|\det \boldsymbol{F}|_{\min}$ vs velocity with multiple local minima.

With the suggested modifications, the algorithm is more robust. All of these four indicators can be applied within this algorithm and they will get the same result, because they share the same minimum zero at the flutter point, as stated in Lemmas 1–4. Moreover, the simple bisection search strategy can be used in the algorithm.

Flutter Eigenvector

The algorithm can locate the flutter point, but the coupled flutter-mode information remains a question. Let us reexamine the flutter equation (10), which could be also taken as an eigenproblem just at the exact flutter point,

$$(\boldsymbol{F} - \lambda_n \boldsymbol{I})\boldsymbol{\eta}_n = 0 \tag{19}$$

because the minimum module eigenvalue of $\boldsymbol{F}$ is $\lambda_n = 0$. The entries in eigenvector $\boldsymbol{\eta}_n$ represent the coupled flutter-mode information. Again, this condition is too critical to be satisfied in numerical application, but the eigenmode at a computed flutter point may serve as an alternative to give the coupled-mode information that leads to flutter instability. Comparisons will be made later between the eigenvector results of the present method and those of the *p-k* method.

To demonstrate and validate the present flutter solution method, a small program is coded for the unified algorithm in MATLAB [19], and four examples will be provided in the next section.

Numerical Examples

All four examples are first solved by the *p-k* or *k* method in MSC/NASTRAN. Then Direct Matrix Abstraction Program statements are applied to extract the generalized mass, stiffness and GAIC matrix from the standard flutter solution sequence of MSC/NASTRAN [17]. The data are then used in the following flutter solutions by the unified algorithm, in which the accuracy is set to 1 ft/s during the bisection search of the flutter speed, but the frequency grid is fixed, for simplicity.

Unrestrained Three-Degree-of-Freedom Airfoil

The first test case is denoted as example HA145A in [17]. The airfoil is attached to a fuselage with free-plunge mode. The structural damping coefficient g is assumed as 0.03, which is equal to a modal damping ratio ζ of 0.015. The frequency band is set as 1–30 rad/s to cover the elastic modes incorporated. The lowest frequency is set to 1 rad/s, which is sufficient to keep the solution away from the nonuniqueness problem caused by the free-plunge mode. A frequency grid of 0.1 rad/s is adopted in the unified algorithm. Good agreement in terms of flutter characteristics between the present method using the four suggested singularity indicators and the *p-k* method is obtained, as shown in Table 1.

Graph of the indicators in the V–ω plane is also obtained. For simplicity, only the graph of indicator $|\det \boldsymbol{F}|$ is shown in Fig. 3. The lowest point indicates flutter, and a bisection search in its neighbor region gives the final result shown in Table 1. Figure 4 shows $|\det \boldsymbol{F}|$-vs-frequency diagrams (indicator diagram) at three different velocities (i.e., 100, 200, and 231.9 ft/s).

Each of these local minimum points, shown in Fig. 4, stands for an aeroelastic mode. There should also be a local minimum point at $\omega = 0$ for the free-plunge mode that is scarcely affected by velocity, but the zero frequency point is excluded from the frequency band analyzed to prevent the nonuniqueness of the singularity. It is seen from Fig. 4 that two aeroelastic modal frequencies decrease as velocity increases, and the elastic plunge modal frequency decreases to the abrupt drop point (i.e., the flutter point), whereas the pitching mode is still not overdamped. This phenomenon is not a classical coupled bending-torsion flutter, and it is sometimes called dynamic divergence [17].

The $|\det \boldsymbol{F}(\omega)|_{\min}$-vs-velocity diagram is shown in Fig. 5, in which the solid line stands for the magnitude of $|\det \boldsymbol{F}(\omega)|_{\min}$ in logarithmic scale and the dashed line stands for the associated frequency in Hz. There are two occurrences of abrupt drops for $|\det \boldsymbol{F}(\omega)|_{\min}$, and the associated frequency changes at the local

Table 1 Flutter characteristics of the unrestrained airfoil

Indicator	V_f, ft/s	ω_f, Hz
$p-k$ method	232.0	1.177
$\lvert\det \boldsymbol{F}\rvert$	231.9	1.194
$\lvert\lambda_n \boldsymbol{F}\rvert$	231.9	1.194
$\sigma_n \boldsymbol{F}$	231.9	1.194
$\text{cond}^{-1} \boldsymbol{F}$	231.9	1.194

Table 2 Flutter characteristics of the BAH wing

Indicator	V_f, ft/s	ω_f, Hz
k method	1056	3.059
$\lvert\det \boldsymbol{F}\rvert$	1057	3.09
$\lvert\lambda_n \boldsymbol{F}\rvert$	1057	3.09
$\sigma_n \boldsymbol{F}$	1057	3.09
$\text{cond}^{-1} \boldsymbol{F}$	1057	3.09

maximum of $|\det \boldsymbol{F}(\omega)|_{\min}$, with the first one indicating the dynamic divergence point and the second one implying the bending-torsion flutter point. Only the instability with lower velocity is presented in Table 1.

Figures 3–5 constitute the main results by the present method with indicator $|\det \boldsymbol{F}|$. Three more examples will be given in the forthcoming discussion to describe the usefulness of other three indicators, respectively.

BAH Wing

This test case is termed example HA145B in [17]. The p-k method is applied to the flutter analysis with no structural damping. The frequency band analyzed is set as 1–400 rad/s for the present method to cover the first 10 modes, and a relatively coarse frequency grid of 1 rad/s is used. The comparison of the flutter characteristics between the present method using four indicators and the p-k method is shown in Table 2.

It is seen from Table 2 that the results are the same for these indicators and almost identical with those obtained by the p-k method. Variation of the second indicator, $|\lambda_n \boldsymbol{F}|$, in the V–ω plane is shown in Fig. 6 and its top view is shown in Fig. 7. Figure 6 shows that with the velocity increasing, the magnitude of the indicator first increases and then drops down around the critical flutter point. In Fig. 7, there are 10 dark strips representing the 10 structural modes used, which is quite similar to the V–ω diagram obtained by the p-k method.

Similarly to the first example, the $|\lambda_n \boldsymbol{F}|$-vs-frequency diagrams are shown in Fig. 8 at three typical velocities (i.e., 200, 600, and 1057 ft/s). As the velocity varies, all the local minimum points on the indicator diagrams change dramatically. At the flutter speed, the first aeroelastic mode becomes overdamped (hence, more stable), whereas the second aeroelastic mode is destabilized to flutter, as shown by the indicator diagrams.

Figure 9 illustrates $|\lambda_n \boldsymbol{F}(\omega)|_{\min}$ and corresponding frequency-vs-velocity diagrams. Again, there is an abrupt drop in the magnitude of $|\lambda_n \boldsymbol{F}(\omega)|_{\min}$ which indicates flutter, and the frequency diagram also has a big change at the maximum of the $|\lambda_n \boldsymbol{F}(\omega)|_{\min}$-vs-velocity diagram.

The eigenvector associated with the minimum module eigenvalue, λ_n, is straightforward for this example, calculated by the present

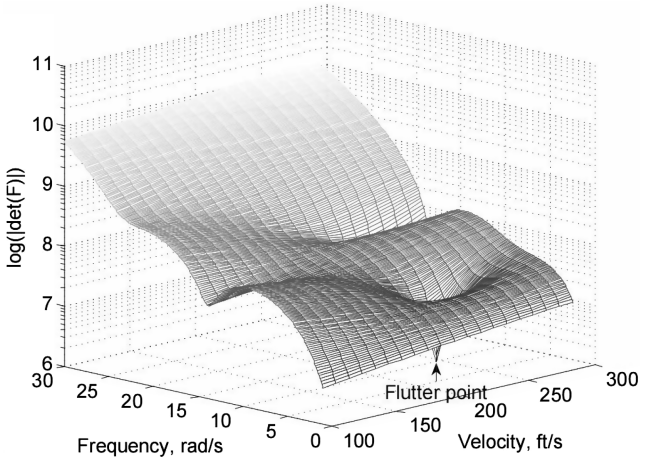

Fig. 3 Diagram of $|\det \boldsymbol{F}|$ in the V–ω plane.

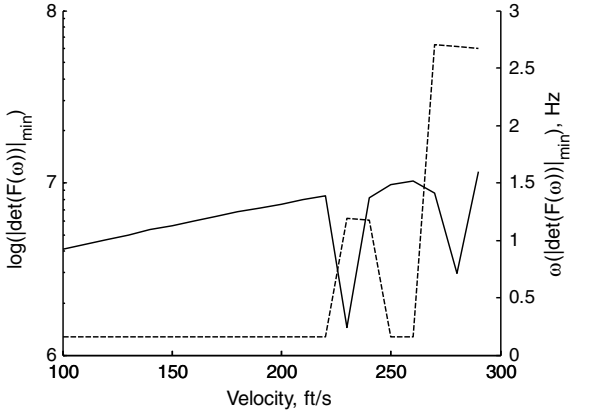

Fig. 5 Diagrams of $|\det \boldsymbol{F}(\omega)|_{\min}$ (solid line) and associated frequency (dashed line) vs velocity.

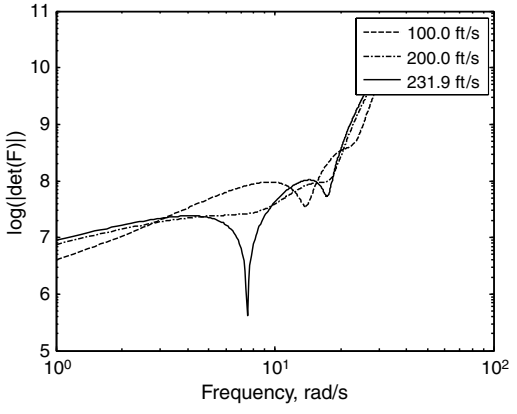

Fig. 4 Diagrams of $|\det \boldsymbol{F}|$ vs ω at 3 different velocities.

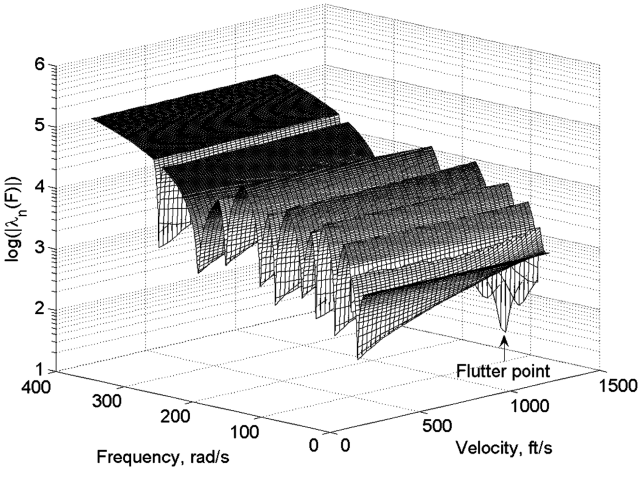

Fig. 6 Diagram of $|\lambda_n \boldsymbol{F}|$ in the V–ω plane.

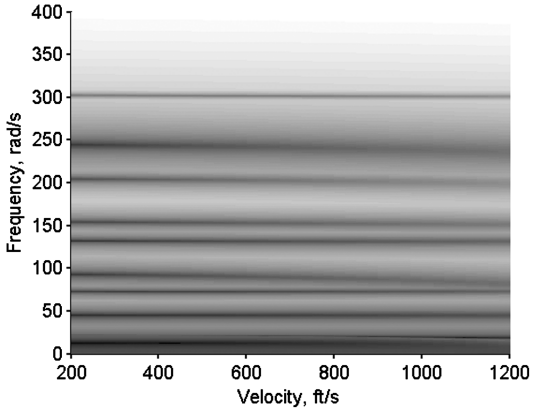

Fig. 7 Top view of Fig. 6: frequency vs velocity.

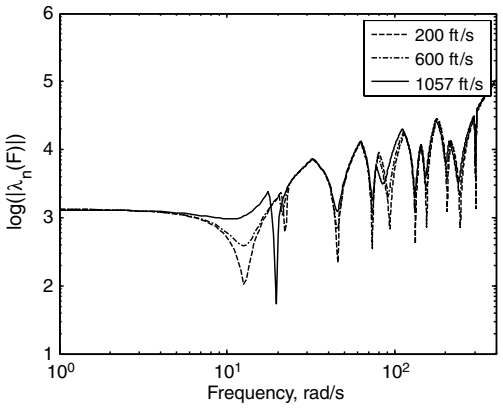

Fig. 8 Diagrams of $|\lambda_n F|$ vs ω at three different velocities.

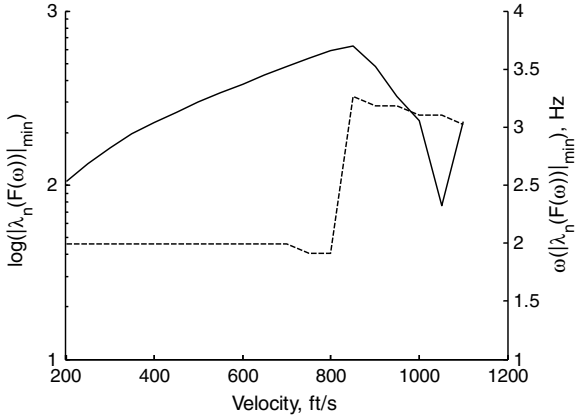

Fig. 9 Diagrams of $|\lambda_n F|_{\min}$ (solid line) and associated frequency (dashed line) vs velocity.

method at 1057 ft/s, which is shown in Fig. 10 and compared with that obtained by the *p-k* method in [17] at 1100 ft/s. It is seen that these two eigenvectors correlate well, except for a slight difference in orientation of the second aeroelastic mode. Note that Fig. 10 only shows the four components with relatively larger magnitude, whereas the other six components are invisible in this graph, because they are rather small in magnitude.

Fifteen-Degree Swept-Back Wing

This test case is called example HA145E in [17], with assumed structural damping $g = 0.0$. The frequency band is set as 1–4000 rad/s to cover the first four structural modes with a coarse frequency grid of 10 rad/s in the present method. (Note: The

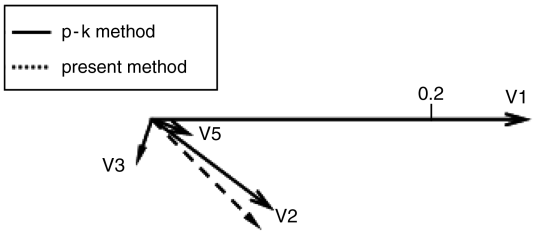

Fig. 10 Flutter eigenvectors comparison between the *p-k* method and the present method.

expected flutter speed should be 491 ft/s from the *V–g* result listed in [17], in which it was mistyped as 483 ft/s.)

Table 3 shows that the flutter speed obtained by the present method is almost identical to the one calculated with the *k* method, except for a slight difference in the flutter frequency, which may be induced by the coarse frequency grid used in the present method. The indicator $\sigma_n \boldsymbol{F}$ is plotted as a function of the *V–ω* plane in Fig. 11, and its top view is shown in Fig. 12. There is also a deep valley indicating the flutter point. Four strips can be observed in Fig. 12, corresponding to the four aeroelastic modes for this example, and the frequency coalescence trend between the first two modes implies the coupled-mode flutter mechanics.

Similarly to the BAH wing, as velocity increases, the first mode becomes overdamped and the second mode is destabilized to flutter, as shown in Fig. 13 for the $\sigma_n(\boldsymbol{F})$-vs-frequency diagrams at 200, 400, and 490 ft/s, and the first two modes coalesce at the flutter point. Figure 14 shows $\sigma_n(\boldsymbol{F}(\omega))_{\min}$ and the corresponding frequency-vs-velocity diagrams. The frequency curve changes abruptly at the occurrence of the maximum of $\sigma_n(\boldsymbol{F}(\omega))_{\min}$, and the consequent valley of $\sigma_n(\boldsymbol{F}(\omega))_{\min}$ indicates flutter.

DAST-ARW I

The last example is the Aeroelastic Research Wing (ARW) adopted by the NASA program Drones for Aerodynamic and Structural Testing (DAST) [20]. DAST-ARW I is a large-aspect-ratio wing model that has two in-plane modes: the first and the second fore–aft wing bending modes. The *p-k* method results and the generalized matrix for flutter solution in MATLAB data format are provided in [20]. The structural damping assumed is $g = 0.01$, for conservativeness. The analysis frequency band is 10–700 rad/s with an interval of 1 rad/s for the present method. Table 4 shows the flutter results obtained by the *p-k* method compared with those obtained by the present method, using the suggested four indicators.

It is shown in Table 4 that the results are identical for the four indicators, and they agree well with the results by the *p-k* method. For this test case, the indicator $\text{cond}^{-1}(\boldsymbol{F})$ is shown in Fig. 15 as a function of the *V–ω* plane, and its top view is shown in Fig. 16.

The deepest valley on the $\text{cond}^{-1}(\boldsymbol{F})$ surface, shown in Fig. 15, indicates flutter, and only a few frequency strips can be identified from Fig. 16. It seems that eigenvalue degeneration occurs to the $\text{cond}^{-1}(\boldsymbol{F})$-vs-frequency diagrams shown in Fig. 17 as velocity increases, which is actually caused by the overdamped second mode vanishing in the indicator diagrams.

There are two local minimum points, respectively, corresponding to the two in-plane modes, in Fig. 17 that are scarcely influenced by

Table 3 Flutter characteristics of the 15 deg swept-back wing

Indicator	V_f, ft/s	ω_f, Hz
$p-k$ method	491.2	113.2
$\lvert\det \boldsymbol{F}\rvert$	489.8	114.75
$\lvert\lambda_n \boldsymbol{F}\rvert$	489.8	114.75
$\sigma_n \boldsymbol{F}$	489.8	114.75
$\text{cond}^{-1}\boldsymbol{F}$	489.8	114.75

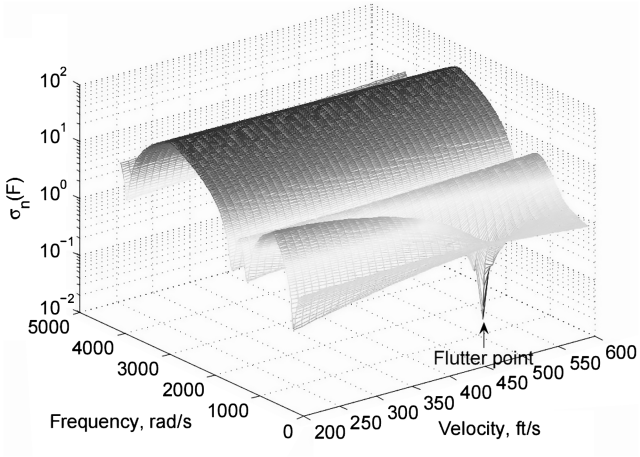

Fig. 11 Diagram of $\sigma_n(F)$ in the V–ω plane.

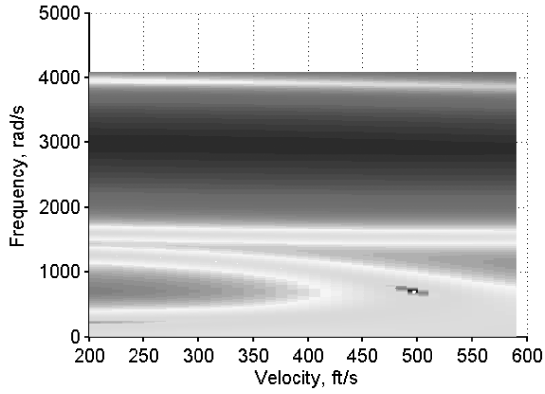

Fig. 12 Top view of Fig. 11: frequency vs velocity.

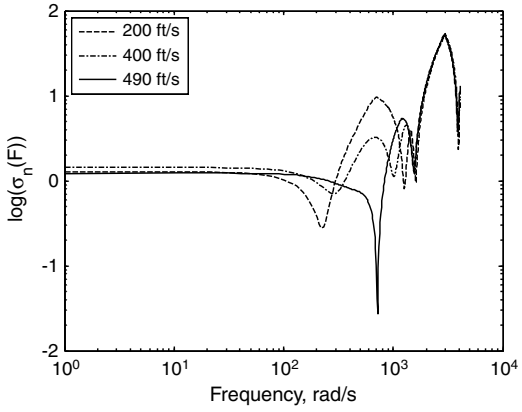

Fig. 13 Diagrams of $\sigma_n(F)$ vs ω at three different velocities.

the velocity, neither for their magnitudes nor their frequencies. Note that the first one is rather close to the singularity in magnitude, which is expected to be a global minimum for $\text{cond}^{-1}(\boldsymbol{F})$ at this frequency, and the present method would fail to get the flutter point, using all the four suggested indicators, if no damping is considered.

Table 4 Flutter characteristics of DAST-ARW I

Indicator	V_f, ft/s	ω_f, Hz
$p-k$ method	283.3	9.64
$\lvert\det \boldsymbol{F}\rvert$	279.4	9.71
$\lvert\lambda_n \boldsymbol{F}\rvert$	279.4	9.71
$\sigma_n \boldsymbol{F}$	279.4	9.71
$\text{cond}^{-1}\boldsymbol{F}$	279.4	9.71

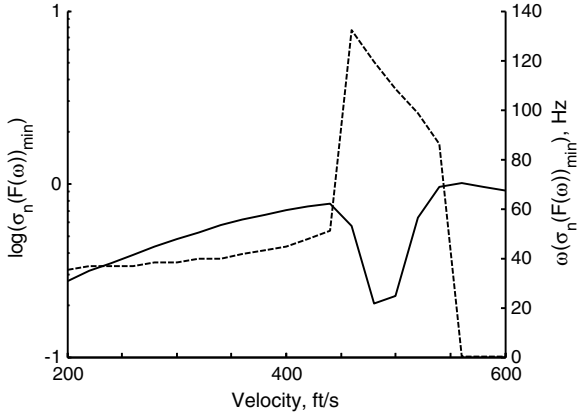

Fig. 14 Diagrams of $\sigma_n(F)_{\min}$ (solid line) and associated frequency (dashed line) vs velocity.

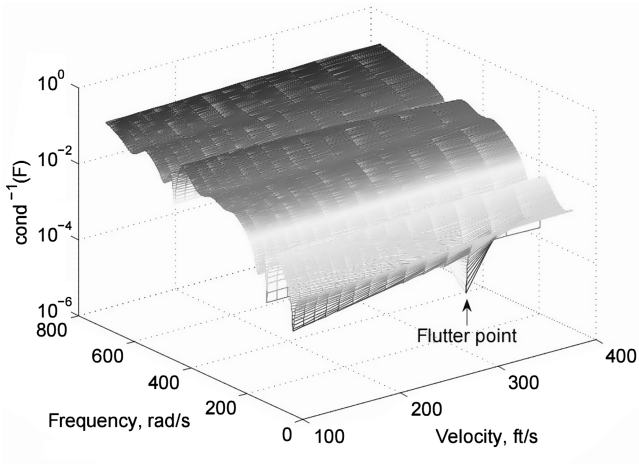

Fig. 15 Diagram of $\text{cond}^{-1}(F)$ in the V–ω plane.

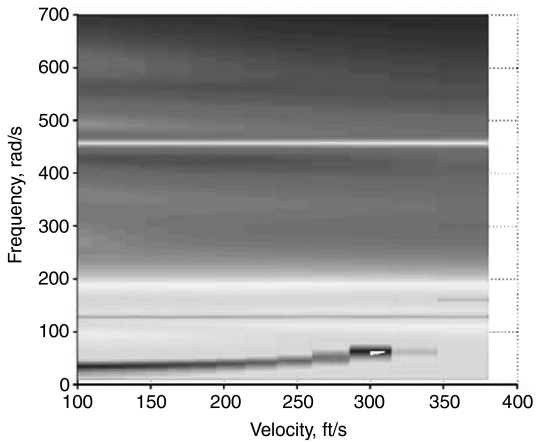

Fig. 16 Top view of Fig. 15.

The $\text{cond}^{-1}(\boldsymbol{F}(\omega))_{\min}$ and its frequency-vs-velocity diagrams are also shown in Fig. 18. Both the magnitude and the frequency of $\text{cond}^{-1}(\boldsymbol{F}(\omega))_{\min}$ change abruptly near the flutter speed. It implies that the flutter indicator for this model is more sensitive to velocity and frequency than other examples in this study. A refined velocity set should be used in the flutter solution for this test case, either by the p-k method or by the present method.

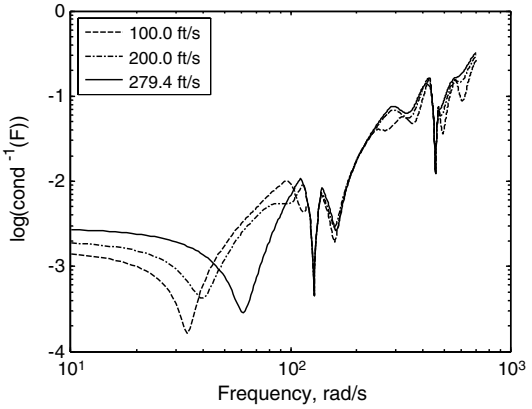

Fig. 17 Diagrams of $\mathrm{cond}^{-1}(F)$ at three different velocities.

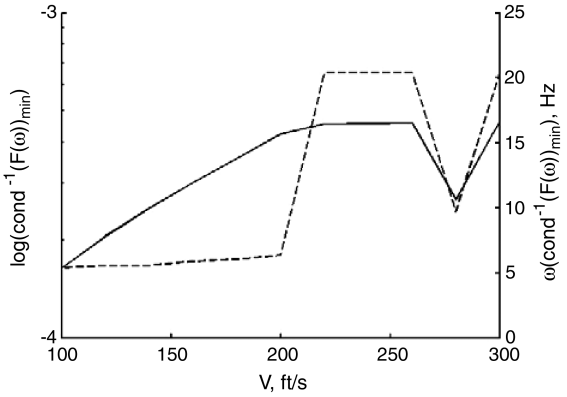

Fig. 18 Diagrams of $\mathrm{cond}^{-1}(F(\omega))_{\min}$ (solid line) and associated frequency (dashed line) vs velocity.

Conclusions

With the discussed clearance procedure, a pertinent conclusion can be reached for the uniqueness of the flutter matrix singularity on the V–ω plane at and inside the flutter boundary under the appropriate assumptions. Four equivalent indicators are suggested to describe the singularity of the flutter matrix, and a unified algorithm is developed to search for the velocity interval that contains the flutter speed by using the local minimum of these indicators along the velocity axis. A primary criterion is proposed to evaluate the effectiveness of such local minimum point, but further testing is still needed in routine applications.

Numerical examples demonstrate that the flutter result is rather accurately obtained by the present method, when compared with calculations by the p-k or k method. The four suggested indicators can give exactly the same flutter solution for each example using the unified algorithm.

The four-indicators-vs-frequency diagrams, at different velocities, can provide physical insight to the dynamic divergence instability and flutter by destabilizing or stabilizing mode. Coupled flutter-mode information extracted by the present method also agrees well with that obtained by the p-k method.

The present method possesses several unique advantages: the four indicators applied are independent of any specific mode explicitly, and thus they are free from mode tracking in the flutter solution procedure. The flutter point is determined by a catastrophe in the magnitude of each specific indicator of the matrix singularity along the velocity axis other than by the traditional V–g diagrams. Finally, one of the most important aspects is that the present method has a potential use in the so-called MDO applications, considering its improvement on the automation and robustness of the flutter solution process compared with the traditional methods.

Acknowledgments

This work was funded by the National Natural Science Foundation of China (grant no. 10672135) and the Program for New Century Excellent Talents in University of China (grant no NCET-04-0965). The authors wish to acknowledge the reviewers for their comments and suggestions that improved this paper.

References

[1] Theodorsen, T., "General Theory of Aerodynamic Instability and the Mechanism of Flutter," NACA Rept. 496, 1935.

[2] Hassig, H. J., "An Approximate True Damping Solution of the Flutter Equation by Determinant Iteration," *Journal of Aircraft*, Vol. 8, No. 11, 1971, pp. 885–889. doi:10.2514/3.44311

[3] Bisplinghoff, R. L., Ashley, H., and Halfman, R. L., *Aeroelasticity*, Addison–Wesley, Reading, MA, 1955.

[4] Dowell, E. H., Crawley, E. F., Curtiss, H. C. Jr., Peters, D. A., Scanlan, R. H., and Sisto, F., *A Modern Course in Aeroelasticity*, edited by E. H. Dowell, 3rd ed., Kluwer Academic, Dordrecht, The Netherlands, 1995.

[5] Chen, P. C., "Damping Perturbation Method for Flutter Solution: The g Method," *AIAA Journal*, Vol. 38, No. 9, 2000, pp. 1519–1524. doi:10.2514/2.1171

[6] Zyl, L. H., "Use of Eigenvectors in the Solution of the Flutter Equation," *Journal of Aircraft*, Vol. 30, No. 4, 1993, pp. 553–554. doi:10.2514/3.46380

[7] Schuster, D. M., Liu, D. D., and Huttsell, L. J., "Computational Aeroelasticity Success, Progress, Challenge," *Journal of Aircraft*, Vol. 40, No. 5, 2003, pp. 843–856. doi:10.2514/2.6875

[8] Afolabi, D., "Flutter Analysis Using Transversality Theory," *Acta Mechanica*, Vol. 103, Nos. 1–4, 1994, pp. 1–15. doi:10.1007/BF01180214

[9] Afolabi, D., Pidaparti, M. V., and Yang, T. Y., "Flutter Prediction Using an Eigenvector Orientation Approach," *AIAA Journal*, Vol. 36, No. 1, 1998, pp. 69–74. doi:10.2514/2.353

[10] Sebastijanovic, N., Ma, T. W., and Yang, T. Y., "Panel Flutter Detection and Control Using Eigenvector Orientation and Piezoelectric Layers," *AIAA Journal*, Vol. 45, No. 1, 2007, pp. 118–127. doi:10.2514/1.22665

[11] Safonov, M. G., Laub, A. J., and Hartmanri, G. L., "Feedback Properties of Multivariable Systems: The Role and Use of the Return Difference Matrix," *IEEE Transactions on Automatic Control*, Vol. 26, No. 1, 1981, pp. 47–65. doi:10.1109/TAC.1981.1102566

[12] Mukhopadhyay, V., and Newsom, J. R., "A Multiloop System Stability Margin Study Using Matrix Singular Values," *Journal of Guidance, Control, and Dynamics*, Vol. 7, No. 5, 1984, pp. 582–587. doi:10.2514/3.19898

[13] Pototzky, A. S., Wieseman, C. D., Hoadley, S. T., and Mukhopadhyay, V., "Development and Testing of Methodology for Evaluating the Performance of Multi-Input/Multi-Output Digital Control Systems," NASA TM 102704, 1990.

[14] Mason, G. S., and Berg, M. C., "Robustness Analysis of a Multirate Flutter Suppression System," *Journal of Guidance, Control, and Dynamics*, Vol. 16, No. 5, 1993, pp. 922–926. doi:10.2514/3.21102

[15] Banerjee, J. R., "Flutter Characteristics of High Aspect Ratio Tailless Aircraft," *Journal of Aircraft*, Vo1. 21, No. 9, 1984, pp. 733–736. doi:10.2514/3.45022

[16] Lillico, M., Butlert, R., Banerjee, J. R., and Guo, S., "Aeroelastic Optimization of High Aspect Ratio Wings Using an Exact Dynamic Stiffness Matrix Method," AIAA Paper 94-4401, 1994.

[17] Rodden, W. P., and Johnson, E. H., *MSC/NASTRAN Aeroelastic Analysis User's Guide*, Ver. 68, MacNeal-Schwendler, Los Angeles, 1994.

[18] Rudin, W., *Real and Complex Analysis*, McGraw–Hill, New York, 1966.

[19] *MATLAB User's Guide*, Ver. 5.3, MathWorks, Inc., Natick, MA, 1999.

[20] Padula, S. L., Alexandrov, N., and Green, L. L., "MDO Test Suite at NASA Langley Research Center," AIAA Paper 96-4028, 1996.